

Comparison of ice adhesion measured with centrifugal and pushing ice adhesion tests

Kamil Khan, Niklas Kandelin, Jarno Jokinen, Heli Koivuluoto*

Materials Science and Environmental Engineering, Faculty of Engineering and Natural Sciences, Tampere University, Korkeakoulunkatu 6, 33720 Tampere, Finland

ARTICLE INFO

Keywords:

Ice adhesion tests
Centrifugal ice adhesion test (CAT)
Pushing ice adhesion test (PAT)
Finite element modelling
Stress Distributions
Aluminium alloys
Flame sprayed Polyethylene (FS PE)

ABSTRACT

Ice accretion and especially ice adhesion greatly influence the performance of different surfaces, materials and structures in many industrial applications, e.g., in aviation, energy and transportation. To reduce ice adhesion, surface engineering plays a crucial role in developing sustainable solutions by tailoring the surface properties. The number of studies on improving and developing anti-icing surfaces and coatings are continuously increasing. Ice adhesion testing methods are used for evaluating de-icing capability of materials and coatings. However, the characterization of ice adhesion strength using standard methods is still lacking. In this research, we focus on investigation of ice adhesion of aluminium alloys and flame sprayed polyethylene coatings with two different ice adhesion test methods: centrifugal ice adhesion test (CAT) and pushing ice adhesion test (PAT). The aim is to compare these test methods using similar ice accretion method and ice type on tested surfaces. An impact ice as a form of mixed glaze ice was accreted by using supercooled water droplets in the icing wind tunnel. This mimics natural ice formation in outdoor conditions. Ice adhesions measured with CAT were higher compared to PAT, which indicates importance to find test specific criteria for ice adhesion levels and icephobicity indicators. Moreover, coated surfaces showed lower ice adhesion, below 100 kPa, with both methods showing their potential as icephobic coatings to be used in de-icing applications. Ice adhesion tests were modelled using finite element method to analyse their stress distributions. Wettability and surface roughness were also evaluated to correlate surface and material properties to icing performance.

1. Introduction

Atmospheric icing is a serious concern and causing several challenges to various industrial sectors. A few examples of many problems caused by icing are safety issues and energy losses e.g., in aircrafts (Yuan et al., 2025), wind turbines (Tarhan and Çil, 2021), marine vessels (Dehghani-Sanij et al., 2017) and transmission lines (Merrill and Feltes, 2006). In addition, icing has a detrimental impact on operational activity, efficiency and reliability of industry, transportation, energy distribution and infrastructure (Koivuluoto et al., 2017). Anti-icing and de-icing methods are used to prevent ice accretion and remove ice from surfaces (Liao et al., 2015). Often, it is necessary to use combinations of anti-icing and de-icing methods for ice removal because there are not available any specific mitigation methods that can eliminate all the risks caused by icing and cold conditions (Rekviene et al., 2024).

Low ice adhesion surfaces have been developed globally for delaying freezing or resisting ice adhesion. For example, icephobic surfaces have been developed by using flame spray method with different coating

design such as dense coatings as well as porous coatings to make slippery liquid impregnated porous surfaces (SLIPS) (Koivuluoto et al., 2020). SLIPS have also been made recently with low-pressure cold spray coating process for anti-icing purposes (Khammas et al., 2026). Detailed use of polymer coatings developed by thermal spray method for different applications, particularly anti-icing, has been discussed in a review article (Koivuluoto, 2022). Furthermore, polysiloxane (Zhuo et al., 2021) and fluoropolymers have shown icephobic characteristics (Yang et al., 2011). Magnetic slippery surfaces have been developed to induce liquid-liquid interface and have resulted in extremely low ice adhesions (Irajizad et al., 2019). A composite surface has been fabricated which contained soft and rigid patterned areas which, in turn, promoted ice crack initiation and increased icephobicity (Ibáñez Ibáñez et al., 2025). There has been a significant progress in the development of icephobic surfaces, but still further development is needed to improve surfaces' application specific requirements in harsh outdoor conditions. Different ice adhesion testing methods are required to evaluate ice adhesion strengths in different icing and ice removal conditions to get

* Corresponding author.

E-mail addresses: kamil.khan@tuni.fi (K. Khan), heli.koivuluoto@tuni.fi (H. Koivuluoto).

better understanding of icing performance of different materials and surfaces.

Many icing and ice adhesion testing facilities have developed their own customized test methods due to the lack of standardized icing tests. Typically, ice adhesion or icing test methods are designed for application-oriented aims. Still, significant variation exists in the test design and conditions even for the same methods. The oldest review of ice adhesion tests has been published in 1979 by Sayward (Sayward, 1979), a common standard material such as aluminium, stainless steel or polymer has been proposed for all evaluations and testing should be performed in the identical way for results' comparison. The recent review by Bleszynski and Clark (Bleszynski and Clark, 2021) have divided ice adhesion tests mainly into two testing types to assess ice adhesion on a flat sample. These are a direct mechanical and a centrifugal ice adhesion test. In the direct mechanical test, a mechanical force is used to remove ice from the tested material surface whereas in the centrifugal ice adhesion test, centrifugal forces are subjected into ice causing stresses to detach ice from the surface. A round robin study to summarize ice adhesion results using same surface types and testing temperature ($-8\text{ }^{\circ}\text{C}$) in various ice adhesion testing facilities was conducted by Rehfeld et al. (Rehfeld et al., 2024). However, geometries and dimensions of the tested samples were not identical because of different specifications of test methods. Ice adhesion strength comparison was also reported for vertical shear test at Norwegian University for Science and Technology (NTNU) and centrifugal test at Université du Québec à Chicoutimi, Anti-icing Materials International Laboratory, Canada (AMIL) (Rønneberg et al., 2020). Both impact and mould ice were used for ice adhesion measurements in AMIL and only mould ice was used in NTNU facilities. The results showed visible difference between ice adhesion values and standard deviations obtained with both methods even for the same type of ice under same testing conditions and surface type. Aluminium had higher deviation with vertical shear test while icephobic coatings had higher deviation with centrifugal test. However, the sample size was not same, and the test performed at different facilities might had influenced the overall results.

To address inconsistencies in ice adhesion methods, finite element (FE) analysis has been used to evaluate the stresses during ice detachment from the tested surface. The load or stress is distributed depending on the ice geometry (Huré et al., 2022). When the stress is distributed non-uniformly and concentrated at the applied force point causes toughness fracture, on the other hand, for large ice thickness compared to its length produces uniform stress leading to a stress based fracture (Huré et al., 2022). Recent research has also provided a detailed FE analysis at the ice-substrate interface of horizontal push test and showed that small ice-substrate interface failure is caused by instantaneous ice detachment called as stress dominated while large interface fracture occurs due to gradual crack propagation identified as toughness dominated (Stendardo et al., 2024) (Stendardo et al., 2023). FE analysis for centrifugal ice adhesion test has been performed, which show that maximum stresses of both shear and normal occurs at the ice-substrate interface irrespective of substrate material and coating layer and therefore causing adhesive failure (Koivuluoto et al., 2015). Therefore, it is important to understand stress distribution and concentrations using FE analysis when comparing test methods even under same experimental conditions.

Though several researches have been carried out to evaluate icephobic surfaces and measure ice adhesion strengths, investigating direct comparison of any two methods under similar ice accretion process and ice types are missing. The aim of this study is to show a comprehensive intra-laboratory comparison of two different ice adhesion tests: centrifugal ice adhesion test (CAT) and pushing ice adhesion test (PAT) used for ice adhesion evaluation with impact ice on different surfaces. The experiments were conducted in a controlled testing conditions inside the ice laboratory. FE modelling of both tests was also performed to understand the stress distribution at the ice-substrate interface. In the current research, the same ice accretion and surface preparation

methods were used to evaluate ice adhesion of different aluminium alloys (Al2017, Al6082, Al7075) and flame-sprayed polyethylene (FS PE) coatings on these Al alloys.

2. Experimental procedure

Three Al alloys Al2017 (Al2), Al6082 (Al6), and Al7075 (Al7) supplied by ALUMECO A/S (Denmark) were investigated as as-received and with coated surfaces. Al2017 alloy is mainly Al and 0.46 wt% Si, 4.31 wt% Cu, 0.68 wt% Mn, 0.72 wt% Mg, and 0.04 wt% Zn. Al6082 alloy is mainly Al and 0.9 wt% Si, 0.09 wt% Cu, 0.44 wt% Mn, 0.8 wt% Mg, and 0.09 wt% Zn. Al7075 consists of mainly Al and 0.06 wt% Si, 1.6 wt% Cu, 0.03 wt% Mn, 2.7 wt% Mg, and 5.8 wt% Zn. The compositions of these alloys were given by supplier. FS PE coatings were applied on each type of Al alloy using flame spray process with an oxygen-acetylene flame. Low-density polyethylene (LDPE) powder was used as a feedstock material (Plascoat Systems Limited, The Netherlands). A mean particle size of powder was $150\text{ }\mu\text{m}$ given by supplier. The feedstock powder combined with compressed air as a carrier gas was feed using a Metco 4MP feeder (Oerlikon Metco, Switzerland). Pressures of gases were 4.0 bar and 0.7 bar for oxygen and acetylene, respectively. Spray distance was 325 mm. Al alloy substrates were pre-heated up to the temperature of $155\text{ }^{\circ}\text{C}$ prior to the flame spray processing. Monitoring of the temperature was performed by a thermal imaging camera (Ti300 IR Fusion Technology, FLUKE, USA). Powder was flame sprayed continuously layer by layer, starting with three layers first and followed by three layers more. The flame spray torch speed and step size were 750 mm/s and 5 mm , respectively. Prior to the coating, substrates were grit-blasted with Al_2O_3 grits (Mesh 40) to increase mechanical interlocking and adhesion.

The ice adhesion strength was calculated from an average value of three measurements along with standard deviation for each tested surface. Ice was accreted using the icing wind tunnel (IWiT) shown in Fig. 1 (IWiT at Tampere University (TAU), Finland), which is placed in a cold-climate room (Koivuluoto et al., 2015) (Stenroos, 2015). The selected test temperature was $-10\text{ }^{\circ}\text{C}$, which has been used in several previous

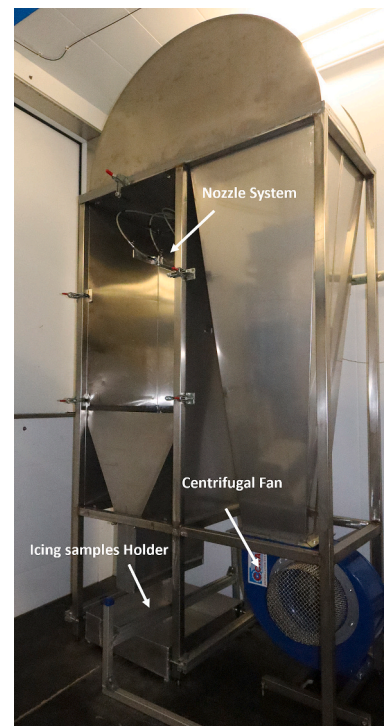


Fig. 1. Experimental setup of impact ice accretion process using IWiT at Tampere University.

studies (Koivuluoto et al., 2015) (Donadei et al., 2020a) (Niemelä-Anttonen et al., 2018) (Khammas and Koivuluoto, 2022) (Aktaş et al., 2025). Deionized water with purity II, purified with Milli-DI Water Purification System (MilliporeSigma, The United States) was sprayed in the IWIT through air atomizing nozzles and accelerated to 25 m/s before hitting the sample surface. The supercooled water droplets accrete ice mimicking how it occurs in nature. The water droplet size was 20–30 μm . The droplet size and speed were measured using HiWatch HR2 (Oseir Ltd., Finland) diagnostic camera with the cold condition optimized model using a uniform laser backlight with the camera to detect the water droplet in-flight properties. The ice was accreted on the sample area as 30 \times 30 mm and ice thickness was targeted as 10 mm. Samples with accreted ice were kept in the same cold conditions ($-10\text{ }^\circ\text{C}$) approximately 16 h before testing. The same ice type and size was used in both ice adhesion tests.

Two ice adhesion testers, CAT and PAT were used. In CAT, ice removal is caused by centrifugal force during the rotation of the sample with an accelerated rotating speed. In PAT, force is coming from the tip of the force gauge contacting the ice and pushing till the removal of the ice. The centrifugal force F is shown in Eq. 1.

$$F = m_{ice}r\omega^2 \quad (1)$$

where m_{ice} is the ice mass, r is the radius and ω is the angular frequency. The fixed acceleration sensor, located in the CAT protective dome, records the angular velocity of an ice detachment. The rotating blade (supporting plate) has a sample attached with one side and a counter-balance weight on the other side to reduce vibration effect during rotation. It is made of aluminium and is 4 mm in thickness. PAT has fixed sample position on the sample stage which can be adjusted both up/down and left/right in relation with the tip. PAT is operated by rotating the wheel manually which creates force probe movement. Force probe acts as a pusher to push ice from the surface. The pusher is made from steel with size of 20 mm diameter, and it is located at 1 mm height from the ice-surface interface. The sample (aluminium plate) thickness is 2 mm in both CAT and PAT. Schematics of CAT and PAT are shown in Fig. 2. The average shear stress τ (average of three parallel samples) given in Eq. 2 was used to calculate ice adhesion strength τ in both CAT and PAT.

$$\tau = \frac{F}{A} \quad (2)$$

where F is the force and A is the iced area. The adhesion reduction factor (ARF) was also calculated using the following Eq. 3 modified from (Laforte and Beisswenger, 2005) which is the average ice adhesion strength as-received surfaces divided by the average ice adhesion strength of FS PE coated surfaces.

$$ARF = \frac{\tau_{as-received}}{\tau_{FS\ PE\ coated}} \quad (3)$$

Static contact angles (CA) were measured with a droplet shape analyzer (DSA100, KRÜSS Scientific, Germany) using the ultra-high purity water (MilliQ, Millipore Corporation, USA). CA values were

determined using the standard sessile-drop method. The measurements were carried out in a controlled environment with an average temperature of $+23\text{ }^\circ\text{C}$ and a humidity level of $50 \pm 2\%$. Each sample underwent nine measurements, where a 5 μL water droplet was placed on the sample surface.

Surface analysis was further carried out using an optical profilometer (Alicona Infinite Focus G5, Alicona Imaging GmbH, Austria) to investigate the effect of surface roughness on ice adhesion. Samples were cleaned for 3 min with ethanol using an ultrasonic cleaner before measurements. The focused area for measurements was 10 mm \times 10 mm at the center position of the sample. The surface roughness parameters chosen were S_a (average height of selected area) and S_{10z} (10-point height of selected area). All measurements were carried out at 5 \times magnification.

3. Finite element modelling

Three-dimensional FE models were made for analysing the CAT and PAT stress distributions. The CAT and PAT models are shown in Fig. 3. FE models were performed using commercial software Abaqus/Standard 2021 (Dassault Systemes, France). The PAT and CAT models included the ice block, sample (aluminium plate) and aluminium supporting plate. In addition, the pusher is modelled in the PAT model. All materials were modelled as linear elastic. The materials properties are shown in Table 1. Material density was only used in the CAT model due to the acceleration-based loading.

The interaction of ice and plate was modelled using tie constraint, which restricted relative motion between them. Similarly, the plate hole and supporting plate were tied. The plate and supporting plate other surfaces in contact had frictionless surface to surface contact. The similar type of contact was also modelled between the pusher and ice in the PAT model. The pusher end, opposite to the contact surface, was made rigid. The pusher end rotations and displacements, excluding the load direction, were restricted. The concentrated force with the value of 134 N was defined in the same location. The force value was based on the PAT experiment providing the highest force. All displacements at the bottom of the supporting plate were restricted in the PAT model. The CAT model boundary conditions were attached to the supporting plate end where displacements were restricted. The rotational body force was used in the CAT model. The value of the angular frequency used in analysis was 544.58 rad/s. The angular frequency was taken from CAT experiments for same as-received aluminium alloy that providing the maximum force for PAT analysis. All parts in both models were meshed using reduced integrated 8-noded solid elements (C3D8R). Typical element dimensions were 0.5 mm in the plate and ice, 1 mm in the pusher and 2 mm in the support plate.

4. Results and discussion

4.1. Modelling of CAT and PAT

Stress distributions are important for understanding the difference in

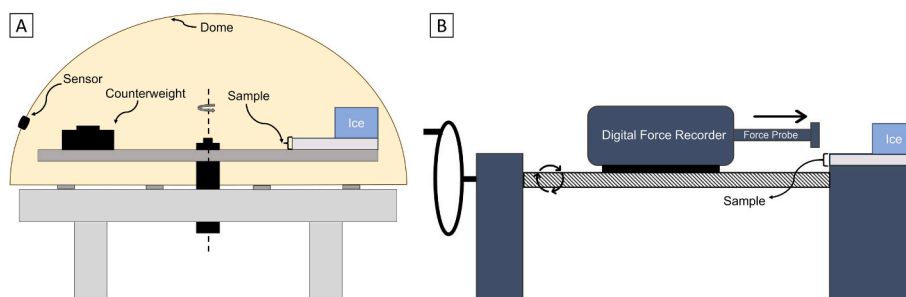


Fig. 2. Schematics of (A) centrifugal ice adhesion test (CAT) and (B) pushing ice adhesion test (PAT).

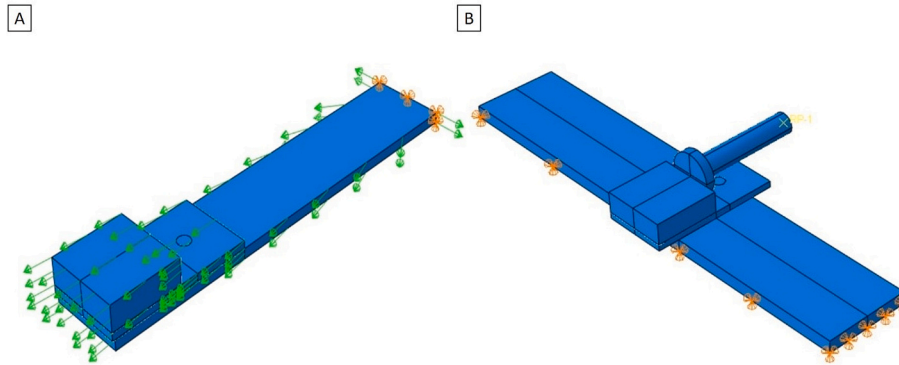


Fig. 3. The FE models of (A) CAT and (B) PAT.

Table 1
Material properties for finite element analyses (Koivuluoto et al., 2015) (Gammon et al., 1983) (MMPDS-03, 2006).

Material	E [GPa]	ν [-]	ρ [kg/m ³]
Aluminium	71	0.33	2700
Steel	210	0.3	-
Ice	9,332	0.325	919

ice adhesion testing methods. For that reason, PAT and CAT tests were analyzed using FE models. Figs. 4 and 5 show shear (S23) and peel (S22) stress distributions and concentrations at the ice-substrate interface for CAT and PAT methods, respectively. Same stresses are also presented as line plots in Fig. 6. Line plot's horizontal axis presents the distance from the ice front, where the highest stresses exist, in the experimental force direction. Line plots are shown at the ice edge and in the middle in the width direction. Ice adhesion strength (Eq. 2) is based on the same shear stress as shear stress (S23) at the interface provided by FE analyses. Peel stress (S22) describes the stress distribution of peeling ice off from the interface. The ice-substrate stresses, shown in Figs. 4 and 5, are based on experimentally obtained maximum forces. Practically, stress distributions provided by analysis are directionally proportional to experimental force due to use of linear elastic material and frictionless contact. The usage of other experimental force values would change the range of minimum and maximum stresses, but distributions would be similar.

Here, the range of experimental force values were from 294 N to 417 N and from 128 N to 134 N for CAT and PAT, respectively.

The shape of shear stress distributions in CAT and PAT seemed to be close. A high shear stress peak is shown in both cases, which reduced by one decimal in few millimeters' length. Similar behaviour is shown in the edge and the middle of the ice. The stress concentrations were smaller at the edges and larger in the middle in both cases CAT and PAT. Peel stresses also have a significant peak value. However, peel stresses reduce to negative value, presenting compressive loading instead peeling off, shortly after the concentration. The peel stress distribution had difference between both methods. The effect of force probe or pusher in contact with ice while pushing the ice caused different peel stress distributions around the tip of force probe in PAT. Peel stresses are close to zero in a major part of the interface in the PAT. In CAT, negative peel stresses are also shown roughly 15 mm to 25 mm distance from the stress concentration. Overall stress concentrations, shear and peel, were relatively higher at the ice-substrate interface in CAT (Fig. 4) compared to PAT (Fig. 5). CAT stresses maximums' are practically double to PAT. Peel stress (S22) had higher stress concentrations values than shear stress (S23) in both methods.

Shear and peel stress distributions had high stress concentrations based on the analysis. Stress concentrations were located at the edge of the ice. The ice is modelled as a cuboid, which provides 90-degree angle on the ice edge and to the edge of the interface. This corner is a natural location for high stress concentration, which values are typically

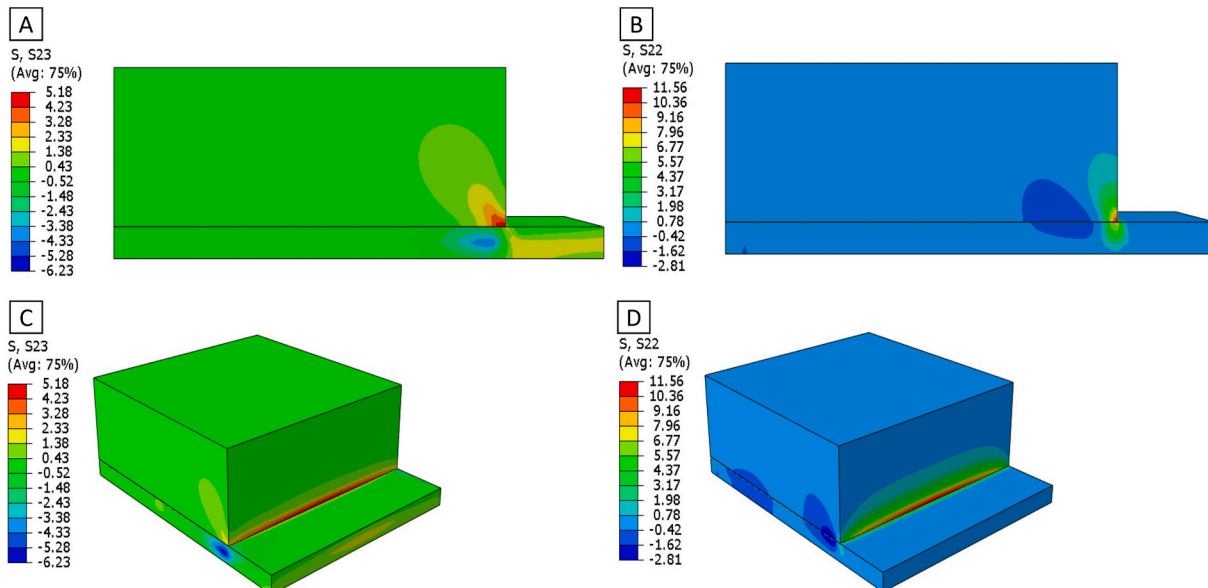


Fig. 4. CAT method out-of-plane shear stress S23 in (A) 2D and (C) 3D and peel stress S22 in (B) 2D and (D) 3D.

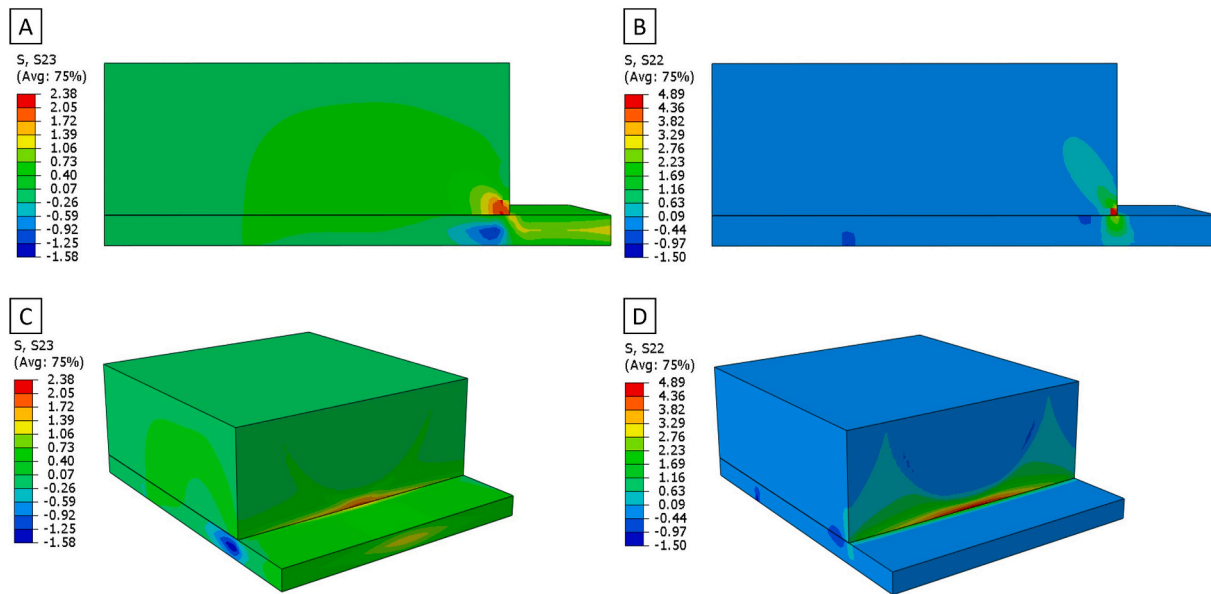


Fig. 5. PAT method out-of-plane shear stress S23 in (A) 2D and (C) 3D and peel stress S22 in (B) 2D and (D) 3D.

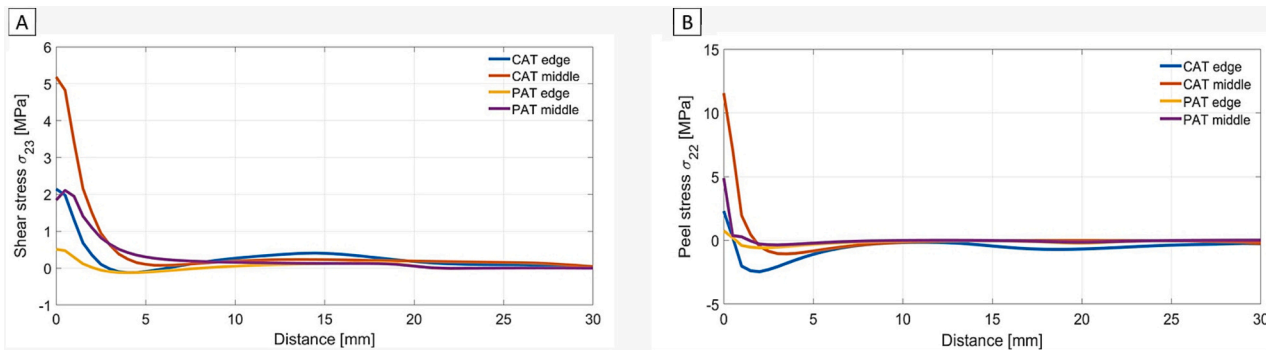


Fig. 6. Shear (A) and peel (B) stress distributions as a line plots. The horizontal axis presents the distance from the stress peak location. Edge and middle presents lines in the loading direction located at the specimen width.

dependent on the element size. In the experimental cases, there might be some rounding, which could reduce peak values.

Shear and peel stress concentration values are reducing significantly in few millimeters' distance. This indicates toughness dominated fracture where detaching would onset and propagate from the stress concentration. In experiments, the detachment of the ice occurred rapidly. This typically refers to a brittle fracture. In future work, an analysis of ice detaching of the substrate could be analyzed using cohesive zone model (CZM). This could provide more understanding of detachment behaviour and differences between PAT and CAT. However, CZM analyses do not come without drawbacks as discussed by (Jokinen et al., 2019). The challenge of CZM analysis is that number of required interface parameters is increasing when fracture toughness for peel and shear modes is required. Naturally, strength values for analyses are also needed for peel and shear. Based on calculated stress values, either peel or shear stress component influence in detaching ice from the substrate cannot be excluded.

The modelling has also validated the non-uniform stress distribution at the interface which is supposed as uniform in Eq. 2 (Work and Lian, 2018). Schulz and Sinapius (Schulz and Sinapius, 2015) has mentioned non-evenly distributed shear stress at the interface despite the fact that centrifugal forces are uniformly distributed in a centrifugal test. They observed that the substrate expansion caused by the centrifugal force significantly altered the shear stress along the interface. Carbon fibre

reinforced polymer due to its high specific stiffness has been proposed as ideally rigid substrate. Nevertheless, previous attempt has been made on stress analysis of ice adhesion but are very limited. Therefore, this study is paving the way for understanding the difference in ice adhesion values of different methods while keeping all other parameters, such as substrate materials and testing conditions, constant. In a nutshell, different loading forces i.e., centrifugal in CAT and linear in PAT influenced both interface stresses as well as overall stress distribution differently and this might be reason for the difference ice adhesion values between them.

4.2. Ice adhesion

Ice adhesion strengths of as-received Al alloys (Al2, Al6, Al7) and FS PE-coated Al alloys (PE-Al2, PE-Al6, PE-Al7) were measured with two different ice adhesion tests, CAT and PAT. Fig. 7 shows ice adhesion strengths measured using both test methods, showing that FS PE-coated surfaces had lower ice adhesions compared to their Al alloy counterparts as expected. Furthermore, the average ice adhesion of FS PE coatings was 67 ± 19 kPa and 54 ± 17 kPa measured with CAT and PAT methods, respectively. Whereas Al alloys had higher ice adhesions compared to polymer coated samples. Average ice adhesion strength of Al alloys was 296 ± 106 kPa measured with CAT whereas it was 111 ± 35 kPa measured with PAT. Summing up, CAT showed higher ice adhesion strength values than those measured with PAT for all coated

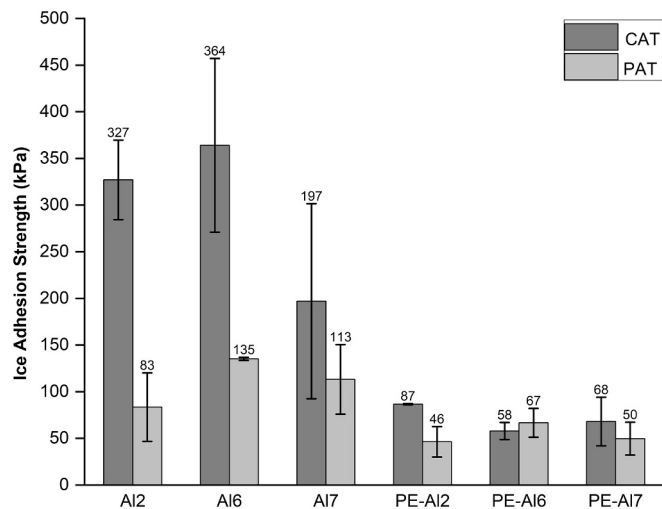


Fig. 7. Ice adhesion strength of as-received Al alloys (Al2, Al6, and Al7) and FS PE-coated (PE-Al2, PE-Al6, and PE-Al7) Al alloys using CAT and PAT methods.

and non-coated samples with only exception of PE-Al6 sample where PAT showed slightly higher ice adhesion (67 kPa) than CAT (58 kPa), but the results were within the standard deviations. The adhesion reduction factors for Al2017, Al6082, and Al7075 were 3.8, 6.3, and 2.9 tested with CAT and 1.8, 2.0, and 2.3 tested with PAT, respectively. All coated samples had increased ARF, indicating coatings' lower ice adhesion compared to their Al alloy substrate counterparts and better icephobicity in de-icing capability.

Previous studies have also reported high ice adhesion strengths for bare Al as 420 ± 27 kPa (Saleema et al., 2011), polished Al as 242.5 ± 26.1 kPa (Arianpour et al., 2016), 640 ± 120 kPa for bare Al and 690 ± 60 kPa for rough Al (Guerin et al., 2016) with CAT method, and for bare Al with PAT method as 261 kPa (Yuan et al., 2020) in different ice test facilities. These values support the high ice adhesion strength of aluminium surfaces observed in this study as well. FS PE coating was selected for this comparative study based on its low ice adhesion properties evaluated earlier (Koivuluoto et al., 2020) (Donadei et al., 2020b). Both CAT and PAT method showed ice adhesion strength below 100 kPa for FS PE-coated surfaces. The ice adhesion strength range between 50 and 100 kPa has been defined as medium-low ice adhesion (Koivuluoto et al., 2020).

Comparing ice adhesion strength of even the same material and surface type across literature cannot be done because testing facilities, e. g., ice adhesion test setup, ice formation, and testing temperature have strong influence on the values. The comparative study based on centrifugal ice adhesion tests at AMIL and TAU facilities using impact ice formed at 15 m/s wind speed showed no consistent ordered sequence for polymeric materials and surfaces (commercial names: Primer, Standox, PTFE tape and PUR C25) (Rehfeld et al., 2024). The stated reason was difference in conditioning times for the ice which was 10 min in AMIL and 17 h in TAU (Rehfeld et al., 2024). The ice adhesion strength has also been influenced by the sample size (Sivakumar and Sundararajan, 2024). In addition, ice type influences on ice adhesion (Kandelin, 2021) (Rønneberg et al., 2019). For this reason, this study kept all influencing parameters same to reduce effect in measured ice adhesion strength and find the causes of difference. Still, the values obtained with CAT and PAT were not the same. The different type of loading in these two test methods could be the reason which was supported by using FE modelling as discussed earlier, showing the difference in stress concentration, components and distribution between them.

In our results, Al6 had the highest ice adhesion strength compared to Al2 and Al7 with both CAT and PAT. The possible reason can be the effect of thermal properties of these as-received Al alloys on the ice adhesion strength. Cohen et al. (Cohen et al., 2016) have studied the

effect of thermal conductivity of substrate on the ice formation and adhesion. However, in their study two superhydrophobic treated substrates were used, copper and polycarbonate, tested at -20 °C for 1 h. Those results have presented that copper substrate due to its high thermal conductivity increased heat transfer during freezing of the water droplets regardless of superhydrophobic coating while polycarbonate which has low thermal conductivity indicated icephobic behaviour by repelling the droplets under same test conditions. Here, our investigation was based on the ice adhesion strengths measured by two different methods in a connection with thermal conductivities of Al alloys. Al6082 has thermal conductivity of 172 W/mK (Alumeco, n.d.-a), which is higher than the thermal conductivities of Al2017 and Al7075 that are 134 W/mK (Alumeco, n.d.-b) and 155 W/mK (Alumeco, n.d.-c), respectively. Therefore, the reason of higher ice adhesion strength of Al6 might be the rapid cooling of supercooled water droplets formed during impact ice and thereby creating a strong adhesion with surface compared to Al2 and Al7. Further in-depth study is needed to justify the influence of thermal conductivity on ice adhesion of Al alloys.

4.3. Surface properties of materials

Static water CA, ice adhesion strengths, and overall ice adhesion of each surface which is the combined average ice adhesions measured with both CAT and PAT methods and surface roughness of each sample are presented in Table 2 for both as-received Al alloys and FS PE-coated Al alloy surfaces. Al2, Al6 and Al7 showed CA less than 90° , while the CAs obtained for PE-Al2, PE-Al6, and PE-Al7 were higher than 90° , reflecting their hydrophobic wetting behaviour.

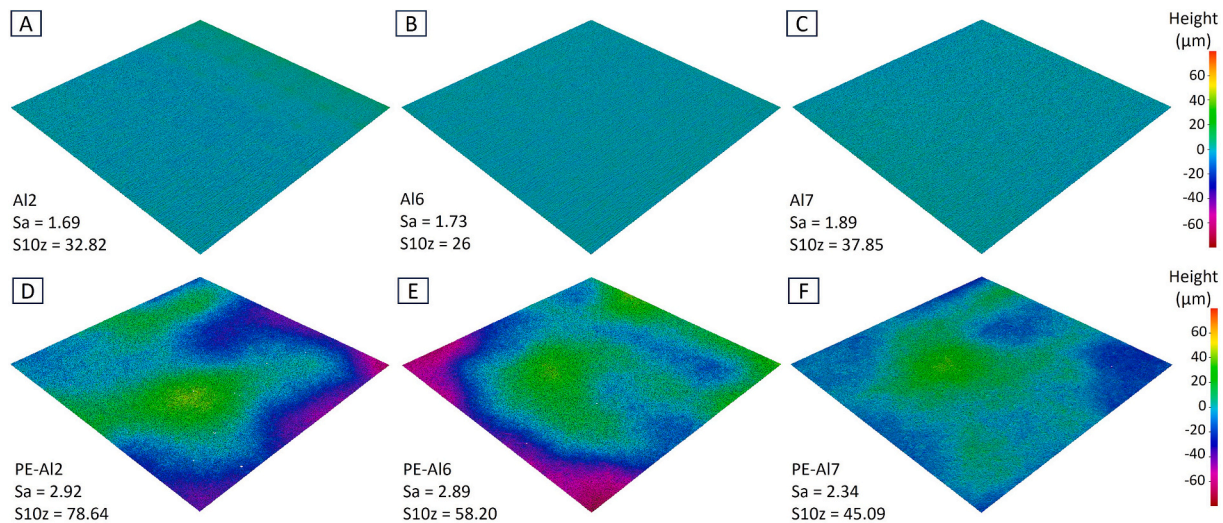
Water molecules affinity with material depends on its surface polarity, which generally increases when polarity increases (Azimi et al., 2013). The number of polar sites in common ceramics and metals are large because of unsaturated coordination at the surface, therefore, they are more likely hydrophilic by making a hydrogen bond with water molecule at the interface (Azimi et al., 2013). Dodiuk et al. (Dodiuk et al., 2012) have studied ice adhesion phenomena in relation with wettability. It has been found that lower ice adhesion can be achieved with higher CA and vice versa. The stated reason was difference in chemical and mechanical interactions of supercooled water droplets with the cold surfaces, high in hydrophilic and low in hydrophobic surfaces. Other studies (Koivuluoto et al., 2017) (Saleema et al., 2011) have also reported higher ice adhesion for bare Al and other hydrophilic surfaces using CAT method.

In addition to wetting behaviour, surface roughness also affected the ice adhesion strength. Coatings were smooth as coated surfaces but not as smooth as as-received Al due to the coating formation by molten droplets, which cooled down after impacting the substrate and affected the surface roughness (Koivuluoto et al., 2020). Both roughness values, Sa and S10z (Fig. 8) were nearly in the same range in similar surfaces, however, coated surfaces had higher roughness than non-coated Al surfaces. Generally, the ice adhesion increases when surface roughness increases (Koivuluoto et al., 2017). Previously, the influence of ice adhesion strength with surface roughness has reported for aluminium and polyurethane (Sivakumar and Sundararajan, 2024). It has been mentioned that increase in roughness level increased the adhesion strength of Al, however, there has not observed similar influence with the polyurethane (Sivakumar and Sundararajan, 2024). The same study has indicated a major increase in adhesion strength at higher roughness level for Al, while polyurethane had slight increase in adhesion at only lower roughness level. Furthermore, surface energy has influenced ice adhesion and it depends on surface nature and chemistry (Cui et al., 2019). Increase in ice adhesion strength with increase in surface free energy of substrates was reported by Ozbay and Erbil (Ozbay and Erbil, 2016). The surface energy of smooth surfaces of Al and PE found in literature was 39 mJ/m^2 and 30.9 mJ/m^2 respectively (Cui et al., 2019). This can explain also why FS PE coated samples had lower ice adhesion strengths with both CAT and PAT even though surface roughness values

Table 2

Contact angle (CA), ice adhesion and surface roughness values of Al alloys and FS PE-coated Al alloys.

Property	Al2	Al6	Al7	PE-Al2	PE-Al6	PE-Al7
CA (°)	77 ± 2	81 ± 7	81 ± 6	93 ± 2	91 ± 1	92 ± 2
CAT - Ice adhesion (kPa)	327 ± 43	364 ± 93	197 ± 105	87 ± 1	58 ± 9	68 ± 26
PAT - Ice adhesion (kPa)	83 ± 37	135 ± 2	113 ± 37	46 ± 16	67 ± 16	50 ± 18
Overall ice adhesion (kPa)	205 ± 40	250 ± 47	155 ± 71	67 ± 9	62 ± 12	59 ± 22
Sa (µm)	1.69	1.73	1.89	2.92	2.89	2.34
S10z (µm)	32.82	26.00	37.85	78.64	58.20	45.09

**Fig. 8.** Surface roughness (A), (B) and (C) represent the roughness profile with Sa and S10z values of as-received Al alloys (Al2, Al6, and Al7) and (D), (E) and (F) correspond to FE PE coated surfaces (PE-Al2, PE-Al6, and PE-Al7).

of FS PE-coated surfaces were higher than as-received Al alloys. It is due to the different surface energy and chemistry of as-received Al and FS PE coated surfaces.

5. Conclusions

Ice adhesion measurements with different techniques and comparison between them require harmonization of testing conditions, which has been done for the first time in the same facility in this study. Two ice adhesion testing methods, CAT and PAT, were used to compare their ice adhesion strengths using the same sample size, testing surfaces and icing conditions. Generally speaking, ice adhesion strength values measured with CAT for all the samples were higher than PAT, except for one coated sample type (PE-Al6), but their values were close to each other. The possible reason for higher values in CAT can be the difference in loading type. This is due to the different design of the test methods which create different levels of stress at the ice-substrate interface during ice removal. FE modelling showed that in both CAT and PAT, the forces influence stress distribution and concentrations at the ice-substrate interface differently. Peel stress had higher concentration than shear stress in both methods. Moreover, when comparing surfaces, PE-coated surfaces had lower ice adhesion strengths than non-coated Al alloys measured with both CAT and PAT methods. Further, both test types recorded ice adhesion strength of PE-coated less than 100 kPa indicating icephobic performance and they also showed hydrophobic behaviour. Lastly, it is understood from this study that even if icing conditions, substrate materials, and geometry are kept the same during testing, still the ice adhesion strength can vary between different test methods.

CRediT authorship contribution statement

Kamil Khan: Writing – original draft, Methodology, Investigation, Formal analysis, Data curation, Conceptualization. **Niklas Kandelin:** Writing – review & editing, Methodology, Investigation, Conceptualization. **Jarno Jokinen:** Writing – review & editing, Formal analysis, Data curation. **Heli Koivuluoto:** Writing – review & editing, Supervision, Resources, Project administration, Methodology, Investigation, Funding acquisition, Conceptualization.

Declaration of competing interest

The authors declare that they have no known competing financial interests or personal relationships that could have appeared to influence the work reported in this paper.

Acknowledgements

Authors would like to thank Mr. Jarkko Lehti and Mr. Anssi Metsähonkala of Tampere University for coating production and helping with the test setup preparation and M.Sc. Ruqaya Khammas of Tampere University for her assistance with icing testing. This research was done partly in the SOUNDofICE project funded by the European Commission through the H2020-FETOPEN-2018-2019-2020-01 (GA number 899352) and partly in the HybriMat project, which is funded by Centre for Economic Development, Transport and the Environments and co-funded by the European Union.

Data availability

Data will be made available on request.

References

- Aktaş, B., Jafari, R., Koivuluoto, H., 2025. Flame-Sprayed ceramic and metallic slippery Liquid-Infused porous and icephobic surfaces. *J. Therm. Spray Technol.* 34, 1843–1854. <https://doi.org/10.1007/s11666-025-01989-3>.
- Alumeco, Metal Wholesaler: Aluminium, Stainless Steel, Copper, Brass and Bronze. n.d. <https://www.alumeco.com/aluminium/sheetsplates/raw-sheetsplates/en-aw-6082/2-x-1000-x-2000-mm/p/10001397/10138957>.
- Alumeco, Metal Wholesaler: Aluminium, Stainless Steel, Copper, Brass and Bronze. n.d. <https://www.alumeco.com/aluminium/sheetsplates/raw-sheetsplates/en-aw-2017a/1-x-1000-x-2000-mm/p/10000313/10005614>.
- Alumeco, Metal Wholesaler: Aluminium, Stainless Steel, Copper, Brass and Bronze. n.d. <https://www.alumeco.com/aluminium/sheetsplates/raw-sheetsplates/en-aw-7075/15-x-1520-x-3020-mm/p/10001397/10001618>.
- Arianpour, F., Farzaneh, M., Jafari, R., 2016. Hydrophobic and ice-phobic properties of self-assembled monolayers (SAMs) coatings on AA6061. *Prog. Org. Coat.* 93, 41–45. <https://doi.org/10.1016/j.porgcoat.2015.12.008>.
- Azimi, G., Dhiman, R., Kwon, H.-M., Paxson, A.T., Varanasi, K.K., 2013. Hydrophobicity of rare-earth oxide ceramics. *Nat. Mater.* 12, 315–320. <https://doi.org/10.1038/nmat3545>.
- Bleszynski, M., Clark, E., 2021. Current ice adhesion testing methods and the need for a standard: a concise review. *Standards* 1, 117–133. <https://doi.org/10.3390/standards1020011>.
- Cohen, N., Dotan, A., Dodiuk, H., Kenig, S., 2016. Thermomechanical mechanisms of reducing ice adhesion on superhydrophobic surfaces. *Langmuir* 32, 9664–9675. <https://doi.org/10.1021/acs.langmuir.6b02495>.
- Cui, W., Jiang, Y., Mielonen, K., Pakkanen, T.A., 2019. The verification of icephobic performance on biomimetic superhydrophobic surfaces and the effect of wettability and surface energy. *Appl. Surf. Sci.* 466, 503–514. <https://doi.org/10.1016/j.apsusc.2018.10.042>.
- Dehghani-Sanj, A.R., Dehghani, S.R., Naterer, G.F., Muzychka, Y.S., 2017. Marine icing phenomena on vessels and offshore structures: Prediction and analysis. *Ocean Eng.* 143, 1–23. <https://doi.org/10.1016/j.oceaneng.2017.07.049>.
- Dodiuk, H., Kenig, S., Dotan, A., 2012. Do self-cleaning surfaces repel ice? *J. Adhes. Sci. Technol.* 26, 701–714. <https://doi.org/10.1163/016942411X575933>.
- Donadei, V., Koivuluoto, H., Sarlin, E., Vuoristo, P., 2020a. Lubricated icephobic coatings prepared by flame spraying with hybrid feedstock injection. *Surf. Coat. Technol.* 403, 126396. <https://doi.org/10.1016/j.surfcoat.2020.126396>.
- Donadei, V., Koivuluoto, H., Sarlin, E., Vuoristo, P., 2020b. Icephobic behaviour and thermal stability of flame-sprayed polyethylene coating: the effect of process parameters. *J. Therm. Spray Technol.* 29, 241–254. <https://doi.org/10.1007/s11666-019-00947-0>.
- Gammon, P.H., Kieft, H., Clouter, M.J., Denner, W.W., 1983. Elastic constants of artificial and natural ice samples by Brillouin spectroscopy. *J. Glaciol.* 29, 433–460. <https://doi.org/10.1017/S0022143000030355>.
- Guerin, F., Laforte, C., Farinas, M.-I., Perron, J., 2016. Analytical model based on experimental data of centrifuge ice adhesion tests with different substrates. *Cold Reg. Sci. Technol.* 121, 93–99. <https://doi.org/10.1016/j.coldregions.2015.10.011>.
- Hurá, M., Olivier, P., Garcia, J., 2022. Effect of Cassie-Baxter versus Wenzel states on ice adhesion: a fracture toughness approach. *Cold Reg. Sci. Technol.* 194, 103440. <https://doi.org/10.1016/j.coldregions.2021.103440>.
- Ibáñez Ibáñez, P.F., Stendardo, L., Ospina, C., Chaudhary, R., Tagliaro, I., Antonini, C., 2025. Discontinuity-enhanced icephobic surfaces for low ice adhesion. *J. Colloid Interface Sci.* 679, 403–410. <https://doi.org/10.1016/j.jcis.2024.09.205>.
- Irajzad, P., Al-Bayati, A., Eslami, B., Shafiqat, T., Nazari, M., Jafari, P., Kashyap, V., Masoudi, A., Araya, D., Ghasemi, H., 2019. Stress-localized durable icephobic surfaces. *Mater. Horiz.* 6, 758–766. <https://doi.org/10.1039/C8MH01291A>.
- Jokinen, J., Kanerva, M., Wallin, M., Saarela, O., 2019. The simulation of a double cantilever beam test using the virtual crack closure technique with the cohesive zone modelling. *Int. J. Adhes. Adhes.* 88, 50–58. <https://doi.org/10.1016/j.ijadhadh.2018.10.015>.
- Kandelin, N., 2021. Icing Factors Affecting Railway Traffic. MSc Thesis. Tampere University, Tampere, Finland. <https://urn.fi/URN:NBN:fi:tuni-202110167632>.
- Khammas, R., Koivuluoto, H., 2022. Durable icephobic slippery Liquid-Infused porous surfaces (SLIPS) using flame- and Cold-Spraying. *Sustainability* 14, 8422. <https://doi.org/10.3390/su14148422>.
- Khammas, R., Jafari, R., Koivuluoto, H., 2026. Icephobic performance of low-pressure cold sprayed PEEK SLIPS. *Cold Reg. Sci. Technol.* 243, 104791. <https://doi.org/10.1016/j.coldregions.2025.104791>.
- Koivuluoto, H., 2022. A review of thermally sprayed polymer coatings. *J. Therm. Spray Technol.* 31, 1750–1764. <https://doi.org/10.1007/s11666-022-01404-1>.
- H. Koivuluoto, C. Stenroos, R. Ruohomaa, G. Bollelli, L. Lusvardi, P. Vuoristo, Research on icing behavior and ice adhesion testing of icephobic surfaces. In: 16th International Workshop on Atmospheric Icing of Structures, IWAIS 2015, Uppsala, Sweden, 2015: pp. 183–188.
- Koivuluoto, H., Stenroos, C., Kylmälahti, M., Apostol, M., Kiilakoski, J., Vuoristo, P., 2017. Anti-icing behavior of thermally sprayed polymer coatings. *J. Therm. Spray Technol.* 26, 150–160. <https://doi.org/10.1007/s11666-016-0501-x>.
- Koivuluoto, H., Hartikainen, E., Niemelä-Anttonen, H., 2020. Thermally sprayed coatings: Novel surface engineering strategy towards icephobic solutions. *Materials* 13, 1434. <https://doi.org/10.3390/ma13061434>.
- Laforte, C., Beisswenger, A., 2005. Icephobic Materials Centrifuge Adhesion Test. In: 11th International Workshop on Atmospheric Icing of Structures, IWAIS 2005, Montreal, QC, Canada, pp. 12–16.
- Liao, R., Zuo, Z., Guo, C., Zhuang, A., Yuan, Y., Zhao, X., Zhang, Y., 2015. Ice accretion on superhydrophobic insulators under freezing condition. *Cold Reg. Sci. Technol.* 112, 87–94. <https://doi.org/10.1016/j.coldregions.2015.01.006>.
- Merrill, H.M., Feltes, J.W., 2006. Transmission icing: a physical risk with a physical hedge. In: 2006 IEEE Power Engineering Society General Meeting, p. 7. <https://doi.org/10.1109/PES.2006.1709619>.
- MMPDS-03, 2006. Metallic Materials Properties Development and Standardization (MMPDS). Federal Aviation Administration.
- Niemelä-Anttonen, H., Koivuluoto, H., Kylmälahti, M., Vuoristo, P., 2018. Thermally Sprayed Slippery and Ice Repellent Surfaces. In: International Thermal Spray Conference 2018, ITSC2018, Orlando, United States.
- Ozbay, S., Erbil, H.Y., 2016. Ice accretion by spraying supercooled droplets is not dependent on wettability and surface free energy of substrates. *Colloids Surf. A Physicochem. Eng. Asp.* 504, 210–218. <https://doi.org/10.1016/j.colsurfa.2016.05.065>.
- Rehfeld, N., Brassard, J.-D., Yamazaki, M., Sakaue, H., Balordi, M., Koivuluoto, H., Mora, J., He, J., Pervier, M.-L., Dolatabadi, A., Asenath-Smith, E., Järn, M., Hou, X., Stenzel, V., 2024. Round-Robin study for ice adhesion tests. *Aerospace* 11, 106. <https://doi.org/10.3390/aerospace11020106>.
- Rekuvieni, R., Saeidiharzand, S., Mäzeika, L., Samaitis, V., Jankauskas, A., Sadaghiani, A.K., Gharib, G., Mugaňli, Z., Koşar, A., 2024. A review on passive and active anti-icing and de-icing technologies. *Appl. Therm. Eng.* 250, 123474. <https://doi.org/10.1016/j.applthermaleng.2024.123474>.
- Rønneberg, S., Laforte, C., Volat, C., He, J., Zhang, Z., 2019. The effect of ice type on ice adhesion. *AIP Adv.* 9, 055304. <https://doi.org/10.1063/1.5086242>.
- Rønneberg, S., Laforte, C., He, J., Zhang, Z., 2020. Comparison of Icephobic Materials through Interlaboratory Studies. In: Mittal, K.L., Choi, C.-H. (Eds.), *Ice Adhesion*, 1st ed. Wiley, pp. 285–324. <https://doi.org/10.1002/9781119640523.ch10>.
- Saleema, N., Farzaneh, M., Paynter, R.W., Sarkar, D.K., 2011. Prevention of ice accretion on aluminum surfaces by enhancing their hydrophobic properties. *J. Adhes. Sci. Technol.* 25, 27–40. <https://doi.org/10.1163/016942410X508064>.
- Sayward, J.M., 1979. Seeking Low Ice Adhesion. U.S. Army Cold Regions Research and Engineering Laboratory, Hanover, NH USA.
- Schulz, M., Sinapius, M., 2015. Evaluation of Different Ice Adhesion Tests for Mechanical Deicing Systems. SAE International, Warrendale, PA. <https://doi.org/10.4271/2015-01-2135>.
- Sivakumar, G., Sundararajan, S., 2024. The effect of surface roughness, stiffness, and size on ice adhesion. *Cold Reg. Sci. Technol.* 225, 104271. <https://doi.org/10.1016/j.coldregions.2024.104271>.
- Stendardo, L., Gastaldo, G., Budinger, M., Pommier-Budinger, V., Tagliaro, I., Ibáñez-Ibáñez, P.F., Antonini, C., 2023. Reframing ice adhesion mechanisms on a solid surface. *Appl. Surf. Sci.* 641, 158462. <https://doi.org/10.1016/j.apsusc.2023.158462>.
- Stendardo, L., Gastaldo, G., Budinger, M., Tagliaro, I., Pommier-Budinger, V., Antonini, C., 2024. Why the adhesion strength is not enough to assess ice adhesion on surfaces. *Appl. Surf. Sci.* 672, 160740. <https://doi.org/10.1016/j.apsusc.2024.160740>.
- Stenroos, C., 2015. Properties of Icephobic Surfaces in Different Icing Conditions, MSc Thesis, Tampere University. <https://urn.fi/URN:NBN:fi:tty-201509241605>.
- Tarhan, C., Çil, M.A., 2021. The use of wind turbines and the problem of icing. *Wind Eng.* 45, 1680–1688. <https://doi.org/10.1177/0309524X21998270>.
- Work, A., Lian, Y., 2018. A critical review of the measurement of ice adhesion to solid substrates. *Prog. Aerosp. Sci.* 98, 1–26. <https://doi.org/10.1016/j.paerosci.2018.03.001>.
- Yang, S., Xia, Q., Zhu, L., Xue, J., Wang, Q., Chen, Q., 2011. Research on the icephobic properties of fluoropolymer-based materials. *Appl. Surf. Sci.* 257, 4956–4962. <https://doi.org/10.1016/j.apsusc.2011.01.003>.
- Yuan, M., Lv, A., Wang, W., Dong, X., Ping, F., 2025. The microphysical properties and processes in in-flight icing: a case study. *Atmos. Res.* 326, 108326. <https://doi.org/10.1016/j.atmosres.2025.108326>.
- Yuan, Y., Wang, L., Liu, G., Liao, R., 2020. Fabrication of ultralow Ice-Adhesion slippery liquid infused porous surfaces on aluminum alloy (7075-T651). *Coatings* 10, 1025. <https://doi.org/10.3390/coatings10111025>.
- Zhuo, Y., Xiao, S., Amirfazi, A., He, J., Zhang, Z., 2021. Polysiloxane as icephobic materials – the past, present and the future. *Chem. Eng. J.* 405, 127088. <https://doi.org/10.1016/j.cej.2020.127088>.